Performance Evaluation and Improvement of Wireless RSSI Based Animal Theft Detection

Thipchinda Prasayasith, Non-member,
Poompat Saengudomlert†, Member, and **Waleed S. Mohammed**, Non-member

ABSTRACT

The use of wireless RSSIs to detect animal theft in an outdoor environment is evaluated. Using simulation experiments, three multilateration techniques for localization are looked at and compared in terms of how accurate they are at detecting things. The last technique is proposed because it requires less computing power. More specifically, the first two techniques are based on setting up an overdetermined set of linear equations with three and two location-related variables, respectively. The proposed technique is the two-variable method simplified when anchor nodes are arranged as a rectangular grid. The investigation of anchor node locations for multilateration is next considered. Finally, a limited motion condition is proposed to reduce the effects of noise in RSSI values on the detection accuracies. Numerical results indicate a trade-off between detection performance improvement and time delay in alarm generation.

Keywords: Wireless Transmission, RSSI, Multilateration, Detection, Simulation Experiment, Performance Evaluation, Performance Improvement

1. INTRODUCTION

Animal thefts, including cattle rustling, are common problems in developing countries that can be mitigated by the use of wireless transmission technologies [1–3]. To help reduce the number of thefts, different types of wireless systems have been used to help locate animals in real time, including the Global Positioning System (GPS) [1], Radio-Frequency IDentification (RFID) [4], Low Power Wide Area Network (LPWAN), including LoRa [2, 3, 5, 6], Sigfox [6–7], and Narrow-Band IoT (NB-IoT) [8].

Using real-time animal localization based on wireless signals, several Internet-of-Things (IoT) systems have been developed to monitor animal locations, analyze their behaviors, and send notifications when abnormal events, including animal thefts, occur [2, 7, 9–11]. While some researchers developed their own IoT platforms, others utilized available platforms such as LoRaWAN [2] and Sigfox [7].

For localization, GPS modules can be used outdoors with sufficient accuracy. However, their costs and relatively high energy consumption motivate researchers to consider alternative solutions [12–14]. LPWAN-based wireless transmissions are attractive for outdoor localization due to their long transmission ranges, low power consumption, and, in several cases, no spectrum license fees [2, 3, 5, 8, 15]. It is worth noting that, while battery lifetimes of GPS-based devices are a few days from hardware experiments [12–14], battery lifetimes of LPWAN-based devices are targeted to be several years [15].

Among several alternative LPWAN technologies, LoRa has been adopted and investigated by a number of researchers [2, 3, 5, 6, 16–19]. LoRa Received Signal Strength Indicator (RSSI) values have been used for localization but with limited accuracies [6, 16–18]. More recently, in [19], data processing algorithms were proposed to improve the accuracies to be comparable to those of GPS. The approach in [19] is to ignore RSSI readings from some anchor nodes when the values appear to be inconsistent with the estimated transmitter location without them.

Besides LoRa signals, localization based on RSSI values from other LPWAN signals has been investigated, including Sigfox signals [6] and NB-IoT signals [8]. Most RSSI-based localization techniques can be categorized into two approaches. The first approach is based on fingerprinting, e.g., [6, 10, 17], where RSSI values at a large number of reference locations are collected and kept in a database to be used later for real-time localization. The second approach is based on multilateration, e.g., [18–19], where the RSSI values are assumed to follow a distance-dependent path loss model created from receive power measurements. The RSSI values are then used to estimate the distances from transmitting anchor nodes, which can then be used to estimate the receiver's location.

While existing works on wireless RSSI-based animal monitoring focus on minimizing the average distance error in localization, this work focuses on the performance evaluation of animal theft detection in terms of detection accuracies, where detection is based on checking whether or not the animal of interest is outside the fences. Using simulation experiments based on

Manuscript received on April 4, 2023; revised on July 3, 2023; accepted on July 13, 2023. This paper was recommended by Associate Editor Kampol Woradit.

The authors are with School of Engineering, Bangkok University.
†Corresponding author: poompat.s@bu.ac.th

Digital Object Identifier: 10.37936/ecti-eec.2023213.251462

a path loss model and additive white Gaussian noise (AWGN) in RSSI values, three RSSI-based multilateration techniques are compared, with the first two being known, e.g., as used in [18–19], and the last one being proposed to reduce the computational complexity for implementation on low-cost devices. In particular, the first two techniques, which will be referred to as three-variable and two-variable methods, are based on setting up an overdetermined set of linear equations with three and two variables, respectively. These sets of equations are then solved to minimize the mean square errors. The proposed technique, referred to as the rectangular grid method, is the two-variable method simplified when anchor nodes are arranged as a rectangular grid. The effects of anchor node locations on detection accuracy are next investigated. Finally, to reduce the effects of noise on RSSI values, a limited animal movement condition is proposed and demonstrated to increase detection accuracies, but with a trade-off between accuracy and time delay.

The remaining sections are as follows: Section 2 describes the system model. Section 3 presents three multilateration techniques for RSSI-based localization. A performance evaluation of RSSI-based animal theft detection is presented in Section 4. Section 5 presents a limited animal motion condition for detection performance improvement and demonstrates a trade-off between accuracy and time delay in detection. Finally, Section 6 summarizes the work.

2. SYSTEM MODEL

Consider wireless transmissions of data signals. Assume that the RSSI value R (in dBm) associated with the transmission distance d (in m) is given by

$$R = R_0 - 10\gamma \log_{10}\frac{d}{d_0} + Z, \tag{1}$$

where d_0 is the reference distance, R_0 is the RSSI value at distance d_0, γ is the loss exponent, and Z is an AWGN term modeled as a Gaussian random variable with mean 0 and variance σ^2.

From RSSI R, we can estimate d by assuming zero error, e.g., as in [18–19], yielding the estimated transmission distance.

$$\hat{d} = d_0 10^{\frac{R_0 - R}{10\gamma}}. \tag{2}$$

Consider N anchor nodes transmitting data packets repeatedly, e.g., every 5 s, to a receiver unit attached to the animal of interest. The receiver unit may be implemented using a microcontroller such as an Arduino or NodeMCU module, which typically has limited memory space and computational power. The animal location can be estimated from the RSSI values associated with the N anchor nodes using one of the multilateration techniques to be discussed in the next section. Fig. 1 illustrates an example scenario with four anchor nodes.

Let $\mathbf{p}_n = (x_n, y_n)$, where $n \in \{1, \ldots, N\}$, denote the location of anchor node n. Let $\mathbf{p}_0 = (x_0, y_0)$ denote the animal's location. Let R_n denote the RSSI value of the signal received from anchor node n. With respect to Eq. (2), let $\hat{d}_n = d_0 10^{\frac{R_0 - R_n}{10\gamma}}$ be the estimated transmission distance be based on R_n.

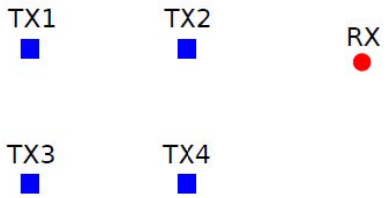

Fig. 1: Example scenario with anchor nodes arranged as a 2×2 grid and denoted by TX1, TX2, TX3, and TX4. The receiver attached to the animal of interest is denoted by RX.

From $\hat{d}_1, \ldots, \hat{d}_N$, multilateration yields the estimated animal location denoted by $\hat{\mathbf{p}}_0$. The details of how $\hat{\mathbf{p}}_0$ is obtained from $\hat{d}_1, \ldots, \hat{d}_N$ are given in the next section for each multilateration method. If the fence area that keeps the animal of interest is denoted by $\mathcal{A}$, then the system detects an animal theft whenever $\hat{\mathbf{p}}_0 \notin \mathcal{A}$.

3. MULTILATERATION TECHNIQUES FOR LOCATION ESTIMATION

3.1 Three-Variable Method

This method is widely used, e.g., [19], and is based on setting up an overdetermined set of equations from which the Minimum Mean Square Error (MMSE) estimate of $\mathbf{p}_0 = (x_0, y_0)$ can be obtained.

More specifically, from the estimated distance $\hat{d}_n$ with respect to anchor node n, we can write

$$(x_0 - x_n)^2 + (y_0 - y_n)^2 = \hat{d}_n^2, \tag{3}$$

which can be written as

$$x_0^2 - 2x_0x_n + x_n^2 + y_0^2 - 2y_0y_n + y_n^2 = \hat{d}_n^2, \tag{4}$$

or equivalently

$$-2x_nx_0 - 2y_ny_0 + (x_0^2 + y_0^2) = \hat{d}_n^2 - (x_n^2 + y_n^2). \tag{5}$$

From the N anchor nodes, we obtain an overdetermined set of N equations shown below.

$$\begin{aligned} -2x_1x_0 - 2y_1y_0 + (x_0^2 + y_0^2) &= \hat{d}_1^2 - (x_1^2 + y_1^2) \\ &\vdots \\ -2x_Nx_0 - 2y_Ny_0 + (x_0^2 + y_0^2) &= \hat{d}_N^2 - (x_N^2 + y_N^2) \end{aligned} \tag{6}$$

The system of equations in Eq. (6) can be written compactly as $\mathbf{Ax} = \mathbf{b}$ with

$$\mathbf{A} = \begin{bmatrix} -2x_1 & -2y_1 & 1 \\ \vdots & \vdots & \vdots \\ -2x_N & -2y_N & 1 \end{bmatrix},$$

$$\mathbf{x} = \begin{bmatrix} x_0 \\ y_0 \\ x_0^2 + y_0^2 \end{bmatrix},$$

$$\mathbf{b} = \begin{bmatrix} \hat{d}_1^2 - (x_1^2 + y_1^2) \\ \vdots \\ \hat{d}_N^2 - (x_N^2 + y_N^2) \end{bmatrix}. \quad (7)$$

From this overdetermined system of equations, the MMSE estimate of $\mathbf{x}$ is [19].

$$\hat{\mathbf{x}} = \left(\mathbf{A}^{\mathrm{T}}\mathbf{A}\right)^{-1}\mathbf{A}^{\mathrm{T}}\mathbf{b}. \quad (8)$$

From the first two components of $\hat{\mathbf{x}}$, we can obtain the estimate $\hat{\mathbf{p}}_0 = (\hat{x}_0, \hat{y}_0)$.

3.2 Two-Variable Method

This method is also widely used, e.g., [18]. Similar to the first technique, with respect to anchor node n, we obtain Eq. (5), which is repeated below for convenience.

$$-2x_n x_0 - 2y_n y_0 + (x_0^2 + y_0^2) = \hat{d}_n^2 - (x_n^2 + y_n^2)$$

Rearranging terms yields

$$2x_n x_0 + 2y_n y_0 = x_0^2 + y_0^2 + x_n^2 + y_n^2 - \hat{d}_n^2. \quad (9)$$

From the N anchor nodes, we obtain the overdetermined set of N equations shown below.

$$\begin{aligned} 2x_1 x_0 + 2y_1 y_0 &= x_0^2 + y_0^2 + x_1^2 + y_1^2 - \hat{d}_1^2 \\ &\vdots \\ 2x_N x_0 + 2y_N y_0 &= x_0^2 + y_0^2 + x_N^2 + y_N^2 - \hat{d}_N^2 \end{aligned} \quad (10)$$

Subtracting the first equation from each of the remaining equations yields $N-1$ equations.[1]

$$\begin{aligned} &2(x_2 - x_1)x_0 + 2(y_2 - y_1)y_0 = \\ &(x_2^2 + y_2^2) - (x_1^2 + y_1^2) - (\hat{d}_2^2 - \hat{d}_1^2) \\ &\vdots \\ &2(x_N - x_1)x_0 + 2(y_N - y_1)y_0 = \\ &(x_N^2 + y_N^2) - (x_1^2 + y_1^2) - (\hat{d}_N^2 - \hat{d}_1^2) \end{aligned} \quad (11)$$

The system of equations can be written compactly as $\mathbf{A}\mathbf{p}_0 = \mathbf{b}$ with

$$\mathbf{A} = \begin{bmatrix} 2(x_2 - x_1) & 2(y_2 - y_1) \\ \vdots & \vdots \\ 2(x_N - x_1) & 2(y_N - y_1) \end{bmatrix},$$

$$\mathbf{b} = \begin{bmatrix} (x_2^2 + y_2^2) - (x_1^2 + y_1^2) - (\hat{d}_2^2 - \hat{d}_1^2) \\ \vdots \\ (x_N^2 + y_N^2) - (x_1^2 + y_1^2) - (\hat{d}_N^2 - \hat{d}_1^2) \end{bmatrix}. \quad (12)$$

From this overdetermined system of equations, the MMSE estimate of $\mathbf{p}_0$, denoted by $\hat{\mathbf{p}}_0 = (\hat{x}_0, \hat{y}_0)$, is computed using [18].

$$\hat{\mathbf{p}}_0 = \left(\mathbf{A}^{\mathrm{T}}\mathbf{A}\right)^{-1}\mathbf{A}^{\mathrm{T}}\mathbf{b}. \quad (13)$$

[1] Instead of the first equation, any other equation can be used to subtract in order to obtain $N-1$ equations.

3.3 Rectangular-Grid Method

This method is proposed for scenarios in which anchor nodes are arranged in a rectangular grid with rows and columns. An example 2×2 grid of anchor nodes for which this method can be applied is shown in Fig. 1. This scenario is discussed in what follows.

Similar to Eq. (10) for the two-variable method, there are four equations from four anchor nodes.

$$\begin{aligned} 2x_1 x_0 + 2y_1 y_0 &= x_0^2 + y_0^2 + x_1^2 + y_1^2 - \hat{d}_1^2 \\ &\vdots \\ 2x_4 x_0 + 2y_4 y_0 &= x_0^2 + y_0^2 + x_4^2 + y_4^2 - \hat{d}_4^2 \end{aligned} \quad (14)$$

By subtracting Eq. (14) between anchor nodes in the same rows, the following equations are obtained:

$$\begin{bmatrix} 2(x_2 - x_1) & 2(y_2 - y_1) \\ 2(x_4 - x_3) & 2(y_4 - y_3) \end{bmatrix} \begin{bmatrix} x_0 \\ y_0 \end{bmatrix} = \begin{bmatrix} (x_2^2 + y_2^2) - (x_1^2 + y_1^2) - (\hat{d}_2^2 - \hat{d}_1^2) \\ (x_4^2 + y_4^2) - (x_3^2 + y_3^2) - (\hat{d}_4^2 - \hat{d}_3^2) \end{bmatrix} \quad (15)$$

Eq. (15) yields two values for x_0 shown below.

$$x_0 = \frac{(x_2^2 + y_2^2) - (x_1^2 + y_1^2) - (\hat{d}_2^2 - \hat{d}_1^2)}{2(x_2 - x_1)}, \quad \frac{(x_4^2 + y_4^2) - (x_3^2 + y_3^2) - (\hat{d}_4^2 - \hat{d}_3^2)}{2(x_4 - x_3)} \quad (16)$$

The average of the two values in Eq. (16) can be used as an estimate of x_0, i.e.,

$$\hat{x}_0 = \frac{1}{2}\left[\frac{(x_2^2 + y_2^2) - (x_1^2 + y_1^2) - (\hat{d}_2^2 - \hat{d}_1^2)}{2(x_2 - x_1)} + \frac{(x_4^2 + y_4^2) - (x_3^2 + y_3^2) - (\hat{d}_4^2 - \hat{d}_3^2)}{2(x_4 - x_3)}\right]. \quad (17)$$

In the same fashion, from anchor node pairs in the same columns, the estimate of y_0 is obtained below.

$$\hat{y}_0 = \frac{1}{2}\left[\frac{(x_3^2 + y_3^2) - (x_1^2 + y_1^2) - (\hat{d}_3^2 - \hat{d}_1^2)}{2(y_3 - y_1)} + \frac{(x_4^2 + y_4^2) - (x_2^2 + y_2^2) - (\hat{d}_4^2 - \hat{d}_2^2)}{2(y_4 - y_2)}\right]. \quad (18)$$

Compared to the first two methods, the computation associated with his method is simpler. Appendix A provides expressions for $\hat{x}_0$ and $\hat{y}_0$ for a general case of $I \times J$ rectangular grid of anchor nodes. The next section compares these three methods in terms of detection accuracy.

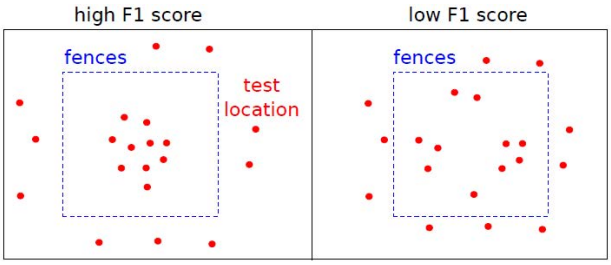

Fig. 2: Dependence of the F1 score on test locations.

4. PERFORMANCE EVALUATION OF ANIMAL THEFT DETECTION

4.1 Performance Measures

Detection performance can be evaluated in terms of the F1 score, which is a measure of accuracy and is equal to the harmonic mean of precision and recall. In particular, let TP, FP, and FN denote the number of true positives, false positives, and false negatives based on a set of detection results from an experiment. The precision, recall, and F1 scores are defined as follows:

$$\text{precision} = \frac{\text{TP}}{(\text{TP}+\text{FP})} \tag{19}$$

$$\text{recall} = \frac{\text{TP}}{(\text{TP}+\text{FN})} \tag{20}$$

$$\text{F1} = \frac{2}{\left(\frac{1}{\text{precision}} + \frac{1}{\text{recall}}\right)} \tag{21}$$

In general, the F1 score depends on the test locations used in the experiment. If most test locations are far from the fences, the F1 score will be high due to low FP and FN values. Otherwise, the F1 score will be low, as illustrated in Fig. 2.

Accordingly, to evaluate the detection performance, animal locations due to random movements are considered where the animal may cross the fences several times, so that both inside and outside random locations are taken into account.

4.2 Test Area and Animal Locations

For simulation experiments, we assume the test area shown in Fig. 3. Note that the areas inside and outside the fences are kept equal. Denote the corner locations of the fences by $(\pm A, \pm A)$. Then, the corners of the test area are $\left(\pm\sqrt{2}A, \pm\sqrt{2}A\right)$. In addition, denote the locations of the 4 anchor nodes by $(\pm L, \pm L)$.

Two models are used to generate random motions. The first model is a simple random walk model in which the animal is assumed to remain where it is or change its location by distance d after each timestep. In particular, if the current location is (x_0, y_0), the next location will be one of the following 5 locations, each with a probability 1/5.

$$(x_0, y_0)\,,\ (x_0+d, y_0)\,,\ (x_0-d, y_0)\,,$$

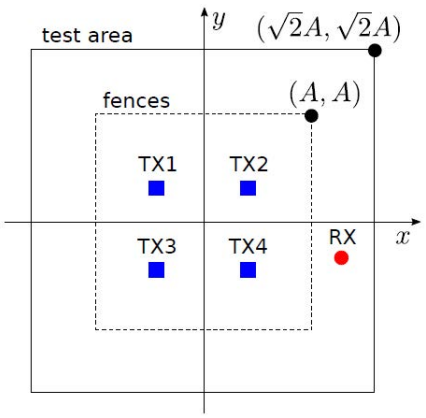

Fig. 3: Test area for simulation experiments with 4 anchor nodes at $(\pm L, \pm L)$.

$$(x_0, y_0+d)\,,\ (x_0, y_0-d) \tag{22}$$

The second model is a random waypoint model in which the animal moves according to the following steps repeatedly.

1. Remain where it is for a random amount of waiting time. Assume that this time is uniformly distributed in $[w_{\min}, w_{\max}]$.
2. Choose the next location and the speed randomly. Then, move to the selected location at the selected speed. Assume that the distance to the next location is uniformly distributed in $[d_{\min}, d_{\max}]$, the direction angle is uniformly distributed in $[0^\circ, 360^\circ]$ and the speed is uniformly distributed in $[s_{\min}, s_{\max}]$.

Note that, for each model, when the next location is outside the test area, the animal remains at the last location within the test area and waits until the next location is within the test area. In this way, the animal may cross the fences but will never leave the test area.

4.3 Setup for Simulation Experiments

Simulation experiments to evaluate the detection performance are conducted using the Octave software [20]. Table 1 lists the simulation parameters together with their default values. In particular, note that each data point in the simulation results is an average of 100 random scenarios, each containing 10^4 timesteps.

Fig. 4 shows example trajectories of the animal motions based on the simple random walk and random waypoint models. It can be seen that, under the simple random walk model, the animal tends to cross the fences more often compared to the random waypoint model. Both models are used to obtain the numerical results in what follows.

4.4 Results of Detection Performances

Fig. 5 shows the values of precision, recall, and F1 score for different values of the noise standard deviation σ for the simple random walk model. Fig. 6 shows the same information for the random waypoint model. As

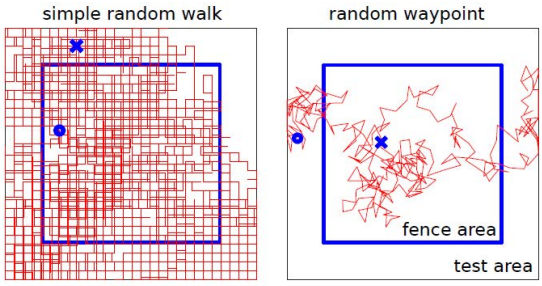

***Fig. 4**: Example animal trajectories based on the simple random walk model and the random waypoint model using the parameters in Table 1. For each trajectory, the initial location is marked as a circle while the final location is a cross.*

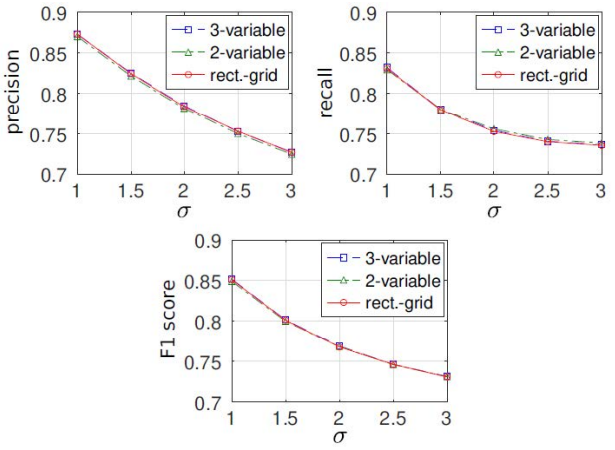

***Fig. 5**: Precision, recall, and F1 score vs. σ for the simple random walk model.*

expected, for both models, as RSSI values contain more noise, i.e., as σ increases, all three performance measures decrease.

Observe from Figs. 5 and 6 that the F1 scores associated with the simple random walk model are consistently lower. This is due to the fact that the animal crosses the fences more often (see Fig. 4) and thus spends comparatively more time near the fences, yielding higher FP and FN values in Eqs. (19) and (20), which in turn lead to a lower F1 score in Eq. (21).

Figs. 5 and 6 also reveal that the detection performances of the three multilateration methods are approximately the same. Given similar performances among these methods, the rectangular-grid method is attractive due to its simpler computation.

4.5 Effects of Anchor Node Locations

Finding appropriate locations for the anchor nodes is considered next. Recall that the 4 anchor node locations are $(\pm L, \pm L)$. Figs. 7 and 8 show the F1 scores for different values of L for the simple random walk and random waypoint models, respectively.

It can be observed that using any value of L in the

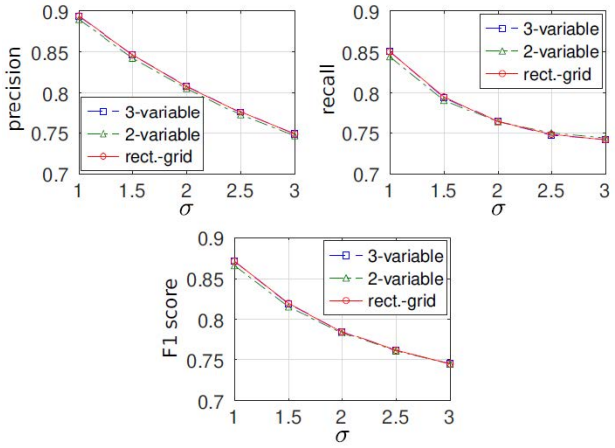

***Fig. 6**: Precision, recall, and F1 score vs. σ for the random waypoint model.*

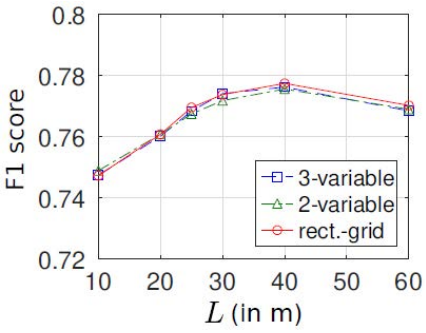

***Fig. 7**: F1 score vs. anchor node location parameter L for the simple random walk model.*

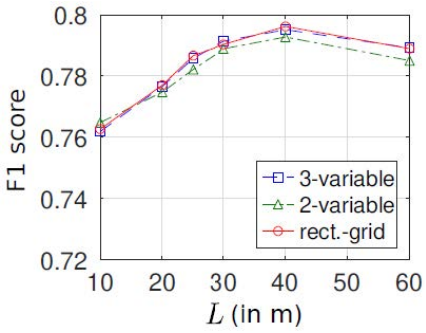

***Fig. 8**: F1 score vs. anchor node location parameter L for the random waypoint model.*

range between 25 m and 60 m yields F1 scores that are higher than using $L < 25$ m. In particular, the value of $L = 40$ m yields the highest F1 scores in Figs. 7 and 8, although the differences among the F1 scores for L in the range from 25 to 50 m are not significant.

Note, however, that using $L > 50$ m may not be practical since the anchor nodes will be located outside the fences. In some cases, the area outside the fences belongs to other people, and it is not possible to deploy equipment on their properties.

On the other hand, using $L < 25$ m leads to

lower F1 scores because the anchor nodes are located more closely to one another, yielding RSSI values that are approximately the same. Since all multilateration methods rely on using the differences among RSSI values from the anchor nodes, the accuracies in terms of the F1 scores are low when the RSSIs are not significantly different.

5. IMPROVEMENT OF DETECTION PERFORMANCE

5.1 Limited Motion Condition

The detection performance can be improved by mitigating the effects of noise in RSSI values. To do so, this section proposes setting a practical condition that the new estimated location cannot be too far from the last estimated location. In other words, the animal motion is limited to being in the neighborhood of the previously estimated location. The specific values of the conditions depend on the animal type of interest and are beyond the scope of this work. In what follows, we demonstrate the approach using limited examples.

More specifically, the new location is first set to a weighted average between the last estimated location and the current estimated location based on the most recent RSSI values. Let $\hat{\mathbf{p}}_0^k$ be the estimated animal location in timestep k. Let $\hat{\mathbf{p}}_0^{\text{RSSI}}$ be the estimated location based on the most recent RSSI values. The estimate in timestep $k+1$ is computed based on the weighted average

$$\alpha\hat{\mathbf{p}}_0^k + (1-\alpha)\hat{\mathbf{p}}_0^{\text{RSSI}}$$

$$= \hat{\mathbf{p}}_0^k + (1-\alpha)\left(\hat{\mathbf{p}}_0^{\text{RSSI}} - \hat{\mathbf{p}}_0^k\right), \quad (23)$$

where α is the weight parameter such that $0 \leq \alpha < 1$. Note that $\alpha = 1$ is not used since it corresponds to using only the old estimated location and not taking into account the updated location based on the RSSI values. With the estimate limited to being within distance D from the last estimate, the estimated location for the timestep $k+1$ can be expressed as

$$\hat{\mathbf{p}}_0^{k+1} = \hat{\mathbf{p}}_0^k + \frac{\min\left((1-\alpha)\left\|\hat{\mathbf{p}}_0^{\text{RSSI}} - \hat{\mathbf{p}}_0^k\right\|, \text{D}\right)}{\left\|\hat{\mathbf{p}}_0^{\text{RSSI}} - \hat{\mathbf{p}}_0^k\right\|}\left(\hat{\mathbf{p}}_0^{\text{RSSI}} - \hat{\mathbf{p}}_0^k\right). \quad (24)$$

Fig. 9 illustrates the limited motion condition as given in Eq. (24). In case 1, the weighted average in Eq. (23) is within distance D of the previous estimate $\hat{\mathbf{p}}_0^k$, and the estimate $\hat{\mathbf{p}}_0^{k+1}$ is therefore set to this weighted average. In case 2, the weighted average in Eq. (23) is further than distance D from $\hat{\mathbf{p}}_0^k$. Accordingly, the estimate $\hat{\mathbf{p}}_0^{k+1}$ is set to be at distance D from $\hat{\mathbf{p}}_0^k$ towards the weighted average in Eq. (23).

5.2 Detection Performances with Limited Motion Condition

Fig. 10 shows the F1 scores for different values of α for the simple random walk model. The value of D is set to 20 meters. Fig. 11 shows the same information for the random waypoint model. Numerical results in Figs. 10 and 11 indicate that using the limited motion condition in Eq. (24) can significantly improve the detection accuracies (in terms of the F1 scores).

Note that, as we keep increasing α, the new location estimate is based more and more on the last estimated lo-

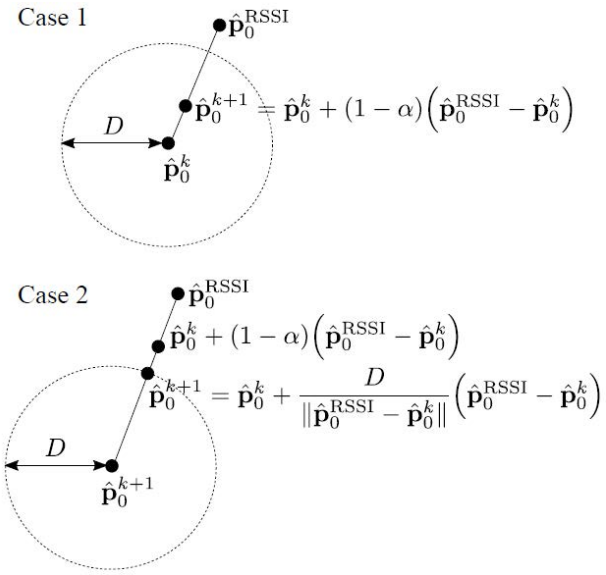

***Fig. 9**: Illustration of the limited motion condition.*

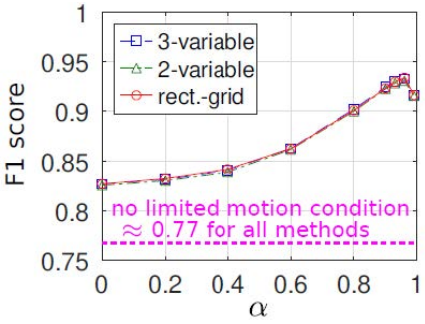

***Fig. 10**: F1 score vs. location update parameter α for the simple random walk model. The F1 score without using the limited motion condition is shown using the dashed line for comparison.*

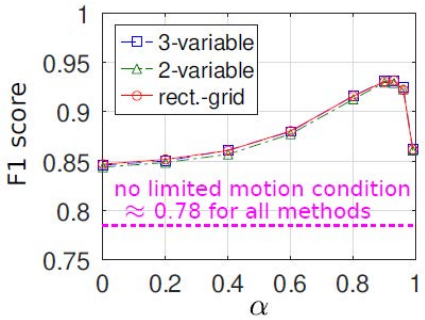

***Fig. 11**: F1 score vs. location update parameter α for the random waypoint model.*

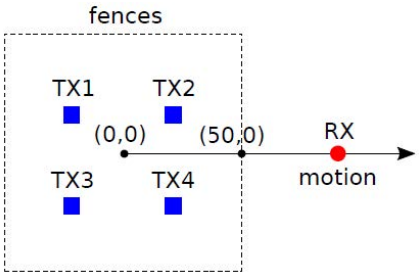

***Fig. 12**: Linear animal motion with a constant speed for delay performance evaluation.*

cation. Surprisingly, the F1 score improvement continues as we increase α as high as 0.9.

As α approaches 1, the expression in Eq. (23) indicates that the new location estimate will be based only on the last estimate and not on the most recent RSSI values. Over time, the new estimate will be incorrect, leading to a significant drop in the F1 score. On the other hand, for $\alpha = 0$, the new estimate is based only on the latest RSSI values, similar to the case of no limited motion. However, with $\alpha = 0$, there are gaps between the F1 scores with and without the limited motion condition due to the fact that the condition sets a distance limit D (regardless of the value of α) from the last estimated location.

While the results seem to indicate that setting α as high as 0.9 is desirable, the next section investigates the time delay of animal theft detection as another performance measure. It will be seen that there is a trade-off between the accuracy performance (in terms of the F1 score) and the delay performance. Accordingly, the parameter α should be chosen by taking into account both accuracy and delay.

More specifically, when α is small (close to 0), a relatively large weight on $\hat{\mathbf{p}}_0^{\text{RSSI}}$ in Eq. (23) results in a quick update on the location estimate based on the most recent RSSI values, leading to a low delay in animal theft detection. On the other hand, when α is large (close to 1), a relatively large weight on the previous estimate ($\hat{\mathbf{p}}_0^k$) in Eq. (23) results in a slow update on the location estimate, leading to a high detection delay.

5.3 Delay Performances of Animal Theft Detection

To evaluate the delay performance in animal theft detection, we consider a linear animal motion as illustrated in Fig. 12. This motion corresponds to a scenario in which the animal of interest is being taken out of the fences. In particular, the animal starts moving from location $(0, 0)$ on a straight line with a constant speed and leaves the fence area at location $(50, 0)$. To accommodate a range of scenarios, the animal's speed is varied from 0.1 m/s to 0.3 m/s. Each simulation scenario consists of 500 timesteps, which are sufficient to cover the motion from location $(0, 0)$ to outside the fences. The time duration between successive timesteps is 5 s (as in Table 1).

The delay in animal theft detection is measured from the moment the animal of interest leaves the fence area to the moment a correct detection (i.e., TP) is generated. To correctly measure delay values without the effects of incorrect detections, noiseless RSSI values are considered in this section. Without noise, all three multilateration methods will correctly identify the animal's location. Therefore, it is sufficient to consider the rectangular-grid method for simulation experiments in this section.

***Table 1**: Parameters for simulation experiments.*

Parameter	Value
Test area:	
A (fence corner)	50 m
L (anchor location)	25 m
RSSI value:	
d_0 (reference distance)	1 m
R_0 (reference RSSI)	-25 dBm
γ (attenuation)	2.5
σ (noise)	2 dB
Animal motion:	
d (random walk step)	1 m
$[w_{\min}, w_{\max}]$ (wait time)	[60, 180] s
$[d_{\min}, d_{\max}]$ (distance)	[10, 20] m
$[s_{\min}, s_{\max}]$ (speed)	[0.1, 0.3] m/s
Timestep:	
Time between detections	5 s
Number of timesteps	10^4
Number of scenarios	100

Fig. 13 shows the time delays in animal theft detection for different values of α and for different speeds. Numerical results show that, for each value of α, the detection delays are approximately the same for all speeds. In addition, the detection delay increases with α for all speeds. In particular, as α increases beyond 0.9, the delay can be excessive, e.g., > 60 s. Since timely discoveries of animal thefts are desirable, using a high value of α for high detection accuracies may not be practical due to excessive detection delays. As a result, a balance must be struck between accuracy and delay.

One approach is to choose α based on a tolerable delay limit, denoted by $T_{\text{d}}^{\max}$. To help identify the value of α chosen in this fashion, Appendix B provides a derivation of an approximate expression of the detection delay given by

$$T_{\text{d}} \approx \frac{\alpha T}{1-\alpha}, \tag{25}$$

where T_{d} denotes the detection delay and T denotes the duration of each timestep, which is 5 s in this work. Note that the delay expression in Eq. (25) is independent of the speed, which is consistent with the results in Fig. 13. Fig. 14 shows the detection delay values from the approximated expression in Eq. (25), which match closely with the simulation results in Fig. 13.

Based on Eq. (25), given the tolerable delay limit $T_{\text{d}}^{\max}$, the value of α for the limited motion condition should be selected such that $T_{\text{d}}^{\max} = \alpha T/(1-\alpha)$, yielding

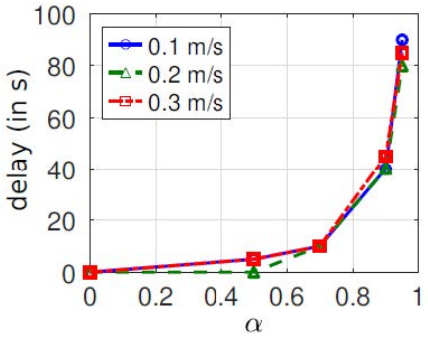

***Fig. 13**: Delay in animal theft detection (in s) vs. location update parameter α for the linear animal motion.*

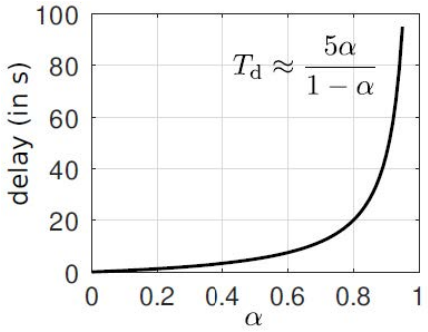

***Fig. 14**: Delay in animal theft detection vs. location update parameter α from the approximated delay expression in Eq. (25) with T = 5 s.*

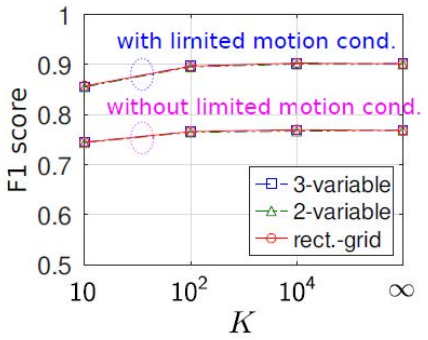

***Fig. 15**: F1 score vs. Rician fading parameter K for the simple random walk model with α = 0.8 for the limited motion condition.*

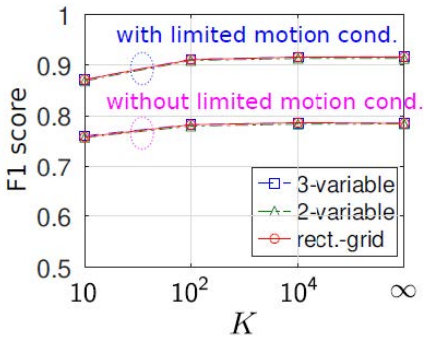

***Fig. 16**: F1 score vs. Rician fading parameter K for the random waypoint model with α = 0.8 for the limited motion condition.*

$$\alpha = \frac{T_{\mathrm{d}}^{\max}}{T_{\mathrm{d}}^{\max} + T} \quad . \tag{26}$$

As a specific example of selecting α, consider $T_{\mathrm{d}}^{\max} = 30$ s and $T = 5$ s. From Eq. (26), the value of α is $30/35 \approx 0.86$. From Figs. 10 and 11, the corresponding F1 scores are approximately 0.91 and 0.93 for the simple random walk and random waypoint models, respectively.

If we reduce the tolerable delay to $T_{\mathrm{d}}^{\max} = 15$ s while keeping $T = 5$ *s*, the value of α in Eq. (26) becomes 15/20 = 0.75. The corresponding F1 scores decrease to approximately 0.89 and 0.91, respectively. This example demonstrates that a smaller detection delay target comes at the price of lower detection accuracies.

5.4 Detection Performances with Multipath Effects

This section investigates the detection performance in the presence of multipath effects in wireless transmissions. For outdoor environments, multipath effects can be modeled using a Rician fading random variable [21], which takes into account a direct transmission path between the transmitter and the receiver as well as additional paths due to reflections, i.e., indirect paths.

More specifically, if X is a random path loss with multipath fading and x_0 is the path loss without fading, then $Y = X/x_0$ has the normalized Rician fading probability density function (PDF) given by

$$f_Y(y) = 2(K+1)\, y e^{-K-(K+1)y^2} I_0\left(2\sqrt{K(K+1)}y\right), \tag{27}$$

where K is the parameter that indicates the ratio between the received power from the direct path and the power from all other indirect paths and I_0 denotes the zeroth-order modified Bessel function of the first kind.

From $Y = X/x_0$, or equivalently $X = x_0 Y$, the power loss X^2 in dB can be written as

$$20\log_{10} X = 20\log_{10} x_0 + 20\log_{10} Y. \tag{28}$$

Therefore, given a randomly generated value of Y, the RSSI value R in Eq. (1) becomes

$$R = R_0 - 10\gamma \log_{10}\frac{d}{d_0} + Z + 20\log_{10} Y, \tag{29}$$

where the last term is added to represent the multipath effects.

Figs. 15 and 16 show the performance of animal theft detection in terms of the F1 score for different values of K, where a larger K means that the direct path carries more signal power. The case of $K = \infty$ refers to having the direct path only, which has been investigated in previous sections. Hence, the values for $K = \infty$ are taken from Figs. 10 and 11. For the limited motion condition, the

location update parameter α is set to 0.8 based on the delay performance analysis in Section 5.3, which suggests that α should be below 0.9.

From Figs. 15 and 16, it can be seen that the detection performance degrades as K decreases due to less signal power on the direct path, i.e., higher multipath effects. In addition, for all values of K, using the limited motion condition can significantly improve the detection performance. Therefore, the proposed limited motion condition is also helpful for scenarios with multipath effects in wireless transmissions.

6. CONCLUSION

This work investigated the performance of animal theft detection using wireless RSSI values through simulation experiments. Three multilateration methods are considered and compared, with the last method being proposed and applicable for scenarios in which anchor nodes are arranged in a rectangular grid with rows and columns. Numerical results indicate no significant differences among the three considered methods, making the rectangular-grid method attractive due to its associated simple computations. The limited motion condition was next considered to improve detection accuracy and was shown to provide significant performance improvements. Then, delay performances were considered, and a trade-off between accuracy and delay performances was demonstrated. Finally, multipath effects were taken into account in terms of Rician fading parameters. Numerical results indicated that the limited motion condition is helpful in improving animal theft detection performance in the presence of multipath effects.

It is recommended that future research involve outdoor testing on a real farm to compare with simulation results. The effects of environmental factors such as terrain type and weather conditions on RSSI-based theft detection should also be investigated. Besides, using other types of sensors, e.g., accelerometers and gyroscopes, to improve the detection performance can be considered. Finally, using machine learning methods, e.g., deep learning and reinforcement learning, to further improve detection performance can be investigated.

APPENDIX A. GENERAL EXPRESSIONS FOR THE LOCATION ESTIMATE IN THE RECTANGULAR-GRID METHOD

For a general case of $I \times J$ rectangular grid of anchor nodes, each node pair in the same row yields one value of $\hat{x}_0$. In particular, if $\mathbf{p}_k = (x_k, y_k)$ and $\mathbf{p}_l = (x_l, y_l)$ are in the same row, the estimate $\hat{x}_0$ from this node pair is as given in Eq. (17), i.e.,

$$\hat{x}_0 = \frac{(x_l^2 + y_l^2) - (x_k^2 + y_k^2) - (\hat{d}_l^2 - \hat{d}_k^2)}{2(x_l - x_k)} . \quad (30)$$

For each of I rows, there are $\binom{J}{2}$ node pairs. Therefore, the number of node pairs whose rows are the same is $I\binom{J}{2}$ in total. Let $\mathcal{R}$ denote the set of anchor node pairs whose rows are the same. For example, in Fig. 1, $\mathcal{R} = \{(1,2),(3,4)\}$. By averaging over all node pairs in $\mathcal{R}$, the overall estimate of $\hat{x}_0$ is given by

$$\hat{x}_0 = \frac{1}{I\binom{J}{2}} \times \sum_{(k,l)\in\mathcal{R}} \frac{(x_l^2 + y_l^2) - (x_k^2 + y_k^2) - (\hat{d}_l^2 - \hat{d}_k^2)}{2(x_l - x_k)} . \quad (31)$$

Similarly, let $\mathcal{C}$ denote the set of anchor node pairs whose columns are the same. For example, in Fig. 1, $\mathcal{C} = \{(1,3),(2,4)\}$. If $\mathbf{p}_k = (x_k, y_k)$ and $\mathbf{p}_l = (x_l, y_l)$ are in the same column, the estimate $\hat{y}_0$ from this node pair is as given in Eq. (18), i.e.,

$$\hat{y}_0 = \frac{(x_l^2 + y_l^2) - (x_k^2 + y_k^2) - (\hat{d}_l^2 - \hat{d}_k^2)}{2(y_l - y_k)} . \quad (32)$$

By averaging over $J\binom{I}{2}$ node pairs in $\mathcal{C}$, the overall estimate of $\hat{y}_0$ is given by

$$\hat{y}_0 = \frac{1}{J\binom{I}{2}} \times \sum_{(k,l)\in\mathcal{C}} \frac{(x_l^2 + y_l^2) - (x_k^2 + y_k^2) - (\hat{d}_l^2 - \hat{d}_k^2)}{2(y_l - y_k)} . \quad (33)$$

APPENDIX B. DERIVATION OF APPROXIMATED DELAY EXPRESSION

Based on the linear motion model, denote the animal's location by $(x_0, 0)$. Without loss of generality, consider the reference location $x_0 = 0$ at time $t = 0$. After k timesteps, where $k \in \{0, 1, 2, \dots\}$, the animal location is given by

$$x_{0,k} = kTs , \quad (34)$$

where $x_{0,k}$ denotes the location after timestep k, s is the animal speed, and T is the timestep, which is 5 s in this work.

With the limited motion condition, the location estimate after timestep k, denoted by $\hat{x}_{0,k}$ with $\hat{x}_{0,0} = 0$, is computed in the noiseless case as follows. Note that we assume D is larger than the distance in each timestep, i.e., $D > Ts$, since the model cannot keep track of the animal otherwise.

$$\begin{aligned} \hat{x}_{0,1} &= \alpha\hat{x}_{0,0} + (1-\alpha)\, x_{0,1} \\ &= \alpha \times 0 + (1-\alpha)Ts \\ &= Ts(1-\alpha) \\ \hat{x}_{0,2} &= \alpha\hat{x}_{0,1} + (1-\alpha)\, x_{0,2} \\ &= \alpha Ts(1-\alpha) + (1-\alpha)2Ts \end{aligned} \quad (35)$$

$$= Ts(2 - \alpha - \alpha^2) \tag{36}$$

$$\hat{x}_{0,3} = \alpha \hat{x}_{0,2} + (1 - \alpha)\, x_{0,3}$$

$$= \alpha Ts(2 - \alpha - \alpha^2) + (1 - \alpha)3Ts$$

$$= Ts(3 - \alpha - \alpha^2 - \alpha^3) \tag{37}$$

In general, after timestep k,

$$\hat{x}_{0,k} = Ts(k - \alpha - \alpha^2 - \ \ldots\ - \alpha^k)$$

$$= Ts\left[k - \frac{\alpha(1 - \alpha^k)}{1 - \alpha}\right]$$

$$\approx Ts\left[k - \frac{\alpha}{1 - \alpha}\right], \tag{38}$$

where the approximation holds for large k since α^k approaches 0 as k increases for $0 < \alpha < 1$.

Let $(B, 0)$ be the fence boundary location, i.e., $B = 50$ m in Fig. 12. From Eq. (34), the animal crosses the fence at timestep k' such that $k'Ts \approx B$ yielding

$$k' \approx \frac{B}{Ts} \ . \tag{39}$$

From Eq. (38), the crossing is detected at timestep k'' such that $Ts\left[k'' - \alpha/(1 - \alpha)\right] \approx B$, yielding

$$k'' \approx \frac{B}{Ts} + \frac{\alpha}{1 - \alpha} \ . \tag{40}$$

From Eqs. (39) and (40), the detection delay is

$$T_{\mathrm{d}} \approx \left(k'' - k'\right) T = \frac{\alpha T}{1 - \alpha} \ , \tag{41}$$

which is as given in Eq. (25).

ACKNOWLEDGMENTS

The first author would like to thank the School of Engineering at Bangkok University, Thailand, for the partial scholarships provided for his graduate study.

REFERENCES

[1] P. K. Mashoko Nkwari, S. Rimer and B. S. Paul, "Cattle monitoring system using wireless sensor network in order to prevent cattle rustling," *2014 IST-Africa Conference Proceedings*, Pointe aux Piments, Mauritius, 2014, pp. 1-10.

[2] O. Dieng, B. Diop, O. Thiare, and C. Pham, "A study on IoT solutions for preventing cattle rustling in african context," *Proceedings of the Second International Conference on Internet of things, Data and Cloud Computing*, Mar. 2017.

[3] O. Dieng, C. Pham, and O. Thiare, "Outdoor Localization and Distance Estimation Based on Dynamic RSSI Measurements in LoRa Networks: Application to Cattle Rustling Prevention," *2019 International Conference on Wireless and Mobile Computing, Networking and Communications (WiMob)*, Oct. 2019.

[4] N. L. Scott, B. Hansen, C. A. LaDue, C. Lam, A. Lai, and L. Chan, "Using an active Radio Frequency Identification Real-Time Location System to remotely monitor animal movement in zoos," *Animal Biotelemetry*, vol. 4, no. 1, Aug. 2016.

[5] L. Liu, Y. Yao, Z. Cao, and M. Zhang, "DeepLoRa: Learning Accurate Path Loss Model for Long Distance Links in LPWAN," *IEEE INFOCOM 2021 - IEEE Conference on Computer Communications*, May 2021.

[6] M. Aernouts, R. Berkvens, K. Van Vlaenderen, and M. Weyn, "Sigfox and LoRaWAN Datasets for Fingerprint Localization in Large Urban and Rural Areas," *Data*, vol. 3, no. 2, p. 13, Apr. 2018.

[7] F. Maroto-Molina et al., "A Low-Cost IoT-Based System to Monitor the Location of a Whole Herd," *Sensors*, vol. 19, no. 10, p. 2298, May 2019.

[8] T. Janssen, R. Berkvens, and M. Weyn, "RSS-Based Localization and Mobility Evaluation Using a Single NB-IoT Cell," *Sensors*, vol. 20, no. 21, p. 6172, Oct. 2020.

[9] L. Nóbrega, A. Tavares, A. Cardoso and P. Gonçalves, "Animal monitoring based on IoT technologies," *2018 IoT Vertical and Topical Summit on Agriculture - Tuscany (IOT Tuscany)*, Tuscany, Italy, 2018, pp. 1-5.

[10] W. Choi, Y.-S. Chang, Y. Jung, and J. Song, "Low-Power LoRa Signal-Based Outdoor Positioning Using Fingerprint Algorithm," *ISPRS International Journal of Geo-Information*, vol. 7, no. 11, p. 440, Nov. 2018.

[11] A. Ur Rehman et al., "Implementation of an Intelligent Animal Monitoring System Using Wireless Sensor Network and IoT Platform," *2022 International Conference on Cyber Resilience (ICCR)*, Dubai, United Arab Emirates, 2022, pp. 1-11.

[12] B. C. Fargas and M. N. Petersen, "GPS-free geolocation using LoRa in low-power WANs," *2017 Global Internet of Things Summit (GIoTS)*, Jun. 2017.

[13] T. Hadwen, V. Smallbon, Q. Zhang, and M. D'Souza, "Energy efficient LoRa GPS tracker for dementia patients," *2017 39th Annual International Conference of the IEEE Engineering in Medicine and Biology Society (EMBC)*, Jul. 2017.

[14] S. Koompairojn, C. Puitrakul, T. Bangkok, N. Riyagoon, and S. Ruengittinun, "Smart tag tracking for livestock farming," *2017 10th International Conference on Ubi-media Computing and Workshops (Ubi-Media)*, Aug. 2017.

[15] K. Mekki, E. Bajic, F. Chaxel, and F. Meyer, "A comparative study of LPWAN technologies for large-scale IoT deployment," *ICT Express*, vol. 5, no. 1, pp. 1–7, Mar. 2019.

[16] W. Choi, Y.-S. Chang, Y. Jung, and J. Song, "Low-Power LoRa Signal-Based Outdoor Positioning Using Fingerprint Algorithm," *ISPRS International Journal of Geo-Information*, vol. 7, no. 11, p. 440, Nov. 2018.

[17] M. Anjum, M. A. Khan, S. A. Hassan, A. Mahmood, H. K. Qureshi, and M. Gidlund, "RSSI Fingerprinting-Based Localization Using Machine Learning in LoRa Networks," *IEEE Internet of Things Magazine*, vol. 3, no. 4, pp. 53–59, Dec. 2020.

[18] K.-H. Lam, C.-C. Cheung, and W.-C. Lee, "New RSSI-Based LoRa Localization Algorithms for Very Noisy Outdoor Environment," *2018 IEEE 42nd Annual Computer Software and Applications Conference (COMPSAC)*, Jul. 2018.

[19] K.-H. Lam, C.-C. Cheung, and W.-C. Lee, "RSSI-Based LoRa Localization Systems for Large-Scale Indoor and Outdoor Environments," *IEEE Transactions on Vehicular Technology*, vol. 68, no. 12, pp. 11778–11791, Dec. 2019.

[20] *GNU Octave: Scientific Programming Language*, octave.org/index.html.

[21] A. Goldsmith, *Wireless Communications*, Cambridge University Press, 2005.

Thipchinda Prasayasith received the B.E. degree in Electronics Engineering from National University of Laos in 2019. In 2023, he received the M. Eng. degree in Electrical and Computer Engineering from Bangkok University, Thailand. His research interests include IoT systems and their applications.

Poompat Saengudomlert obtained the B.S.E. degree in Electrical Engineering from Princeton University, USA, in 1996. He then obtained the S.M. and Ph.D. degrees, both in Electrical Engineering and Computer Science, from Massachusetts Institute of Technology (MIT), USA, in 1998 and 2002 respectively. From 2003 to 2004, he was a Postdoctoral Research Associate in Laboratory of Information and Decision Systems (LIDS) at MIT. From 2005 to early 2013, he was a faculty member (Lecturer, Assistant Professor, and finally Associate Professor) in Telecommunications at Asian Institute of Technology (AIT), Thailand. From May 2013 up to present, he is a Research Scholar and Associate Professor in Telecommunication Engineering at Bangkok University's Center of Research in Optoelectronics, Communication and Computational Systems (BU-CROCCS), Thailand. His research interest includes visible light communications, communication theory, and network optimization.

Waleed S. Mohammed graduated from the Department of Electronics and Electrical Communications, Faculty of Engineering, Cairo University, Giza, Egypt, in 1996 with a major in control systems. In 1997, he joined the Lasers Institute (NILES), Cairo University, as a teaching assistant. He received the M.Sc. degree from the Department of Computer Engineering, Cairo University under the supervision of Prof. Adel El-Nadi and Prof. Ali Fahmy in 1999. In the same year, he joined the College of Optics and Photonics/CREOL, University of Central Florida, Orlando, FL, USA, as a research assistant. In 2001, he received the M.Sc. degree in Optics. He completed his Ph.D. work in 2004 and his thesis was titled "Nano/micro optical elements for mode coupling applications." In 2004, he joined Prof. P.W.E. Smith's Ultra-Fast Photonics Laboratory (UPL), Electrical and Computer Engineering Department, University of Toronto, as a postdoctoral fellow. In 2005, he joined Prof. Li Qian's group at the same university. In 2007, he joined the International School of Engineering, Chulalongkorn University, Bangkok, Thailand, as an instructor in the Nano-Engineering Department. He taught optoelectronics, fundamental of optics, numerical modeling, nano-electronics and research methodology. In September 2010, he joined the School of Engineering, Bangkok University as a research scholar.